
The Space of Transferable Adversarial Examples

Florian Tramèr¹, Nicolas Papernot², Ian Goodfellow³, Dan Boneh¹, and Patrick McDaniel²

¹Stanford University, ²Pennsylvania State University, ³Google Brain

Abstract

Adversarial examples are maliciously perturbed inputs designed to mislead machine learning (ML) models at test-time. Adversarial examples are known to *transfer* across models: a same perturbed input is often misclassified by different models despite being generated to mislead a specific architecture. This phenomenon enables simple yet powerful black-box attacks against deployed ML systems.

In this work, we propose novel methods for estimating the previously unknown *dimensionality* of the space of adversarial inputs. We find that adversarial examples span a contiguous subspace of large dimensionality and that a significant fraction of this space is shared between different models, thus enabling transferability.

The dimensionality of the transferred adversarial subspace implies that the decision boundaries learned by different models are eerily close in the input domain, when moving away from data points in adversarial directions. A first quantitative analysis of the similarity of different models' decision boundaries reveals that these boundaries are actually close in *arbitrary* directions, whether adversarial or benign.

We conclude with a formal study of the *limits* of transferability. We show (1) sufficient conditions on the *data distribution* that imply transferability for simple model classes and (2) examples of tasks for which transferability fails to hold. This suggests the existence of defenses making models robust to transferability attacks—even when the model is not robust to its own adversarial examples.

1 Introduction

Through slight perturbations of a machine learning (ML) model's inputs at test time, it is possible to generate *adversarial examples* that cause the model to misclassify at a high rate [5, 23]. Adversarial examples can be used to craft human-recognizable images that are misclassified by computer vision models [23, 8, 12, 16], software containing malware but classified as benign [13, 26, 9, 10], and game environments that force reinforcement learning agents to misbehave [11, 4, 15].

Adversarial examples often *transfer* between models trained for the same task [23, 8, 18]: despite being generated to evade a specific architecture, they are misclassified by different models. Transferability is a strong obstacle to the secure deployment of ML: an adversary can launch *black-box attacks*, by using a local surrogate model to craft adversarial examples that also mislead the target model [23]. Such surrogate models can be trained even in the absence of training data, and with minimal interaction with the target model [19]. A better understanding of why adversarial examples transfer between models appears necessary for building successful defenses against such attacks.

Adversarial Subspaces. Empirical evidence has shown that, rather than being scattered randomly in small pockets, adversarial examples occur in large, contiguous regions [8, 25]. The dimensionality of these subspaces seems relevant to the transferability problem: the higher the dimensionality, the more likely it is that the subspaces of two models will intersect significantly. Incidentally, the larger the intersection of these subspaces, the harder it is to defend against black-box attacks.

This work directly estimates the dimensionality of these subspaces for the first time. We introduce methods for discovering multiple *orthogonal* adversarial directions and show that these span a multi-dimensional contiguous space of misclassified points. To measure transferability of these subspaces, we experiment on datasets for which diverse model classes attain high accuracy: digit classification [14] and malware detection [1].¹ For a fully-connected network trained on MNIST, we find that on average adversarial examples that transfer lie in a 25-dimensional space.

Transferability of large adversarial subspaces implies that the decision boundaries learned by different models (e.g., an SVM and a neural network) are close in the input domain, when moving away from data points in adversarial directions. We empirically show that models from different hypothesis classes learn decision boundaries that are close in *arbitrary* directions, whether adversarial or benign.

More precisely, we find that when moving into any direction away from the data points, the distance traveled before reaching a model’s decision boundary is on average larger than the distance *separating* the decision boundaries of two models in that direction. Thus, adversarial perturbations that have sufficient magnitude to send data points far over a model’s decision boundary are very likely to transfer to other models with different architectures.

The Limits of Transferability. Given the empirical prevalence of transferability, it is natural to ask whether this can be explained by simple properties of datasets, model classes, or training algorithms. In Section 5, we consider the following informal hypothesis:

If two models achieve low error for some task while also exhibiting low robustness to adversarial examples, these adversarial examples transfer between the models.

This hypothesis is pessimistic: it implies that a model cannot be reasonably secure against adversarial examples transferred from other models (e.g., as is the case for the black-box attacks mentioned earlier) if it is not also robust to its own adversarial examples. Yet, while this hypothesis holds in certain contexts, we show that it is *not* true in the general case.

We derive sufficient conditions on the data distribution that imply a form of the above hypothesis for a set of simple model classes. Namely, we prove transferability of *model-agnostic* perturbations, obtained by shifting data points in the direction given by the difference in class means (in input space). These adversarial examples are by design effective against linear models. Yet, we show, both formally and empirically, that they can transfer to higher-order (e.g., quadratic) models.

However, we exhibit a counter-example to the above hypothesis by building a variant of the MNIST dataset for which adversarial examples fail to transfer between linear and quadratic models. Our experiment suggests that transferability is not an inherent property of non-robust ML models. This suggests that it may be possible to defend against black-box attacks—at least for a subset of possible attacking model classes—despite the targeted model not being robust to its own adversarial examples.

Our Contributions. To summarize, we make the following contributions:

- We introduce methods for finding multiple independent attack directions. These span a contiguous and transferable adversarial subspace of dimensionality that is an order of magnitude larger compared to previous results.
- We perform the first quantitative study of the similarity of models’ decision boundaries and show that models from different hypothesis classes learn decision boundaries that lie very close to one-another in both adversarial and benign directions.
- In a formal study, we identify sufficient conditions for transferability of model-agnostic perturbations, as well as tasks where adversarial example transferability fails to hold.

2 Adversarial Example Generation

Adversaries may seek to alter the behavior of a deployed ML system [2, 21] through manipulations at training time [6] (e.g., by poisoning the data from which model parameters are learned), or at test time (e.g., by finding adversarial examples). In this work, we focus on the latter threat model.

¹We use a balanced subset of the DREBIN dataset, pre-processed using feature selection to have 1,000 features (in lieu of about 500,000). The models we train get over 94% accuracy on this dataset.

Adversarial example crafting techniques usually aim to mislead an ML model into producing either *targeted* misclassifications (i.e., the model predicts a class of the adversary’s choosing) or *untargeted* misclassifications (i.e., the models predicts any class other than the ground truth). We exclusively consider untargeted attack strategies in this work. We begin by introducing some notation.

- x, y A clean input from some domain D and its corresponding label.
- x^* An adversarial input in D . To enforce $x^* \in D$, we either clip all pixels to the range $[0, 1]$ for MNIST, or we round all feature values to a binary value for DREBIN.
- r The perturbation vector added to an input to create an adversarial example: $x^* = x + r$.
- ϵ The magnitude of the adversarial perturbation, i.e., $\epsilon = \|r\|$ for some appropriate norm (we will use the ℓ_1, ℓ_2 and ℓ_∞ norms in this work).
- $J(x, y)$ The loss function used to train an ML model f .

2.1 First-Order Gradient-based Attacks

These attacks find the optimal perturbation under a first-order approximation of the model’s output or loss function. We use the implementations provided by the `cleverhans 1.0` library [17].

Fast Gradient [Sign] Method (FG[S]M). This method proposed in [8] is an efficient way of generating adversarial examples with a fixed ℓ_∞ -norm: $x^* = x + \epsilon \cdot \text{sign}(\nabla_x J(x, y))$.

In our experiments, we also consider variants of this approach that constrain the perturbation using other ℓ_p norms:

$$x^* = x + \epsilon \cdot \nabla_x J(x, y) / \|\nabla_x J(x, y)\| \tag{1}$$

For general ℓ_p norms, we drop the “sign” in the acronym and simply call it the *fast gradient method*.

Jacobian-based Saliency Map Approach (JSMA). This iterative method evaluates the Jacobian matrix of the model f and ranks features in a saliency map that encodes the adversarial goal [20]. A few input features (typically one or two) with high saliency scores are perturbed (i.e., increased to their maximum value) at each iteration, before repeating the process with the modified input.

2.2 Convex Optimization for Piecewise Linear Models

An entirely different approach to finding adversarial examples was proposed by Bastani et al. [3] for the (ubiquitous) case where the model f is a piecewise linear function (here we identify the output of f with the vector of unnormalized log-probabilities preceding the softmax output). Instead of relying on a linear *approximation* of the model’s output, their idea is to restrict the search of adversarial perturbations for an input x to the convex region $Z(x)$ around x on which f is linear.

Let x be a point that f classifies as class s (i.e., $\arg \max f_i(x) = s$). Further let the “target” t be the class to which f assigns the second-highest score. The approach from [3] consists in finding a perturbation r as a solution to a convex program with the following constraints, denoted $C(x)$:

- $x + r \in Z(x)$, which can be expressed as a set of linear constraints (see [3] for more details).
- $\|r\| \leq \epsilon$ (although Bastani et al. focus on the ℓ_∞ norm, any convex norm can be used).
- $f_t(x + r) < f_s(x + r)$.

If all constraints are satisfied, $x + r$ must be misclassified (possibly as another class than the target t).

3 Exploring the Space of Transferable Adversarial Examples

The transferability of adversarial examples is well established in the literature. Our aim here is to evaluate the dimensionality of the adversarial subspace that transfers between models. We use novel techniques to demonstrate how adversarial examples form a contiguous subspace, in over hundreds of dimensions for some inputs. We further evaluate the extent to which the subspace spanned by these adversarial inputs transfers between models.

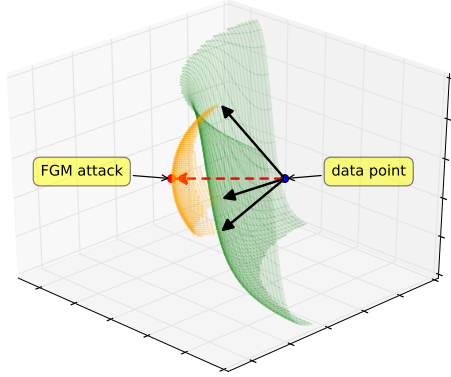


Figure 1: Illustration of the Gradient Aligned Adversarial Subspace (GAAS). The gradient aligned attack (red arrow) crosses the decision boundary. The black arrows are orthogonal vectors aligned with the gradient that span a subspace of potential adversarial inputs (orange).

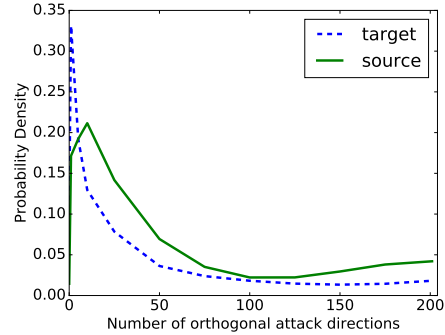


Figure 2: Probability density function of the number of successful orthogonal adversarial perturbations found by the GAAS method on the source DNN model, and of the number of these perturbations that transfer to the target DNN model.

3.1 Finding Multiple Adversarial Directions

The attacks presented in Section 2.1 efficiently compute adversarial examples by taking one or more steps in the *unique* optimal direction under a first-order approximation of the model’s output or loss function. However, we know that adversarial examples form a dense space that is (1) at least two-dimensional [25], and (2) occupies a negligible fraction of the entire input space [23].

This raises the question of how “large” the space of adversarial examples is (which in turn may help us better understand why these examples transfer). We introduce strategies designed to find multiple *orthogonal* adversarial directions for an input x , thus providing an estimate on the dimensionality of the space of adversarial examples.

Our first two techniques iteratively solve some optimization problem with an additional constraint enforcing orthogonality of the solutions. The latter two estimate the dimensionality of the adversarial space more directly, using first-order approximations of the model’s output or loss.

Second-Order Approximations. Consider an analog of the FGM with a second-order approximation of the loss function. That is, we want a perturbation r that solves $\max_{\|r\| \leq \epsilon} g^\top r + \frac{1}{2} r^\top H r$, where $g = \nabla_x J(x, y)$ is the gradient and $H = \nabla_x^2 J(x, y)$ is the Hessian of the loss function.

We can find orthogonal perturbations as follows: Given a first solution r_1 to the above optimization problem, we substitute g and H by $g' := P g$ and $H' := P^\top H P$, where P is a projection matrix onto the space orthogonal to r_1 . The solution r_2 to the updated problem is then orthogonal to r_1 .

Convex Optimization. We suggest an extension to the LP from Bastani et al. [3] (see Section 2.2), for finding orthogonal adversarial directions. After finding a solution r_1 with constraint set $C(x)$, we extend the constraints as $C'(x) := C(x) \wedge (r_1^\top r = 0)$, and solve the convex program again to find a new solution r_2 orthogonal to r_1 . This process is iterated until the constraints are unsatisfiable.

Gradient Aligned Adversarial Subspace (GAAS). This technique directly computes the dimensionality of the adversarial subspace under a first-order approximation of the loss function. For an input x , we search the space of perturbations r (with $\|r\|_2 \leq \epsilon$) that results in a significant increase in loss, i.e., $J(x + r, y) \geq J(x, y) + \gamma$, for a $\gamma > 0$. We can recast this as the problem of finding a maximal set of orthogonal perturbations r_1, r_2, \dots, r_k , satisfying $\|r_i\|_2 \leq \epsilon$ and $r_i^\top \nabla_x J(x, y) \geq \gamma$.

To define the maximal orthogonal set, we introduce the following result:

Lemma 1. *Given $g \in \mathbb{R}^d$ and $\alpha \in [0, 1]$. The maximum number k of orthogonal vectors $r_1, r_2, \dots, r_k \in \mathbb{R}^d$ satisfying $\|r_i\|_2 \leq 1$ and $g^\top r_i \geq \alpha \cdot \|g\|_2$ is $k = \min \left\{ \left\lfloor \frac{1}{\alpha^2} \right\rfloor, d \right\}$.*

Model	Method	Transfer Rate	# of dirs on f_{src}	# of dirs on f_{target}
DNN	Second-Order	95%	1.00	0.95
	Convex Opti.	17%	2.58	0.45
	GAAS	94%	44.28	24.87
CNN	GAAS	69%	15.18	2.24

Table 1: Comparison of techniques for finding multiple orthogonal perturbations on MNIST. We report: (1) the transfer rate of each method when used to find a single adversarial direction, (2) the average number of (successful) orthogonal adversarial perturbations found on the source model f_{src} and (3) the average number of these perturbations that transfer to model f_{target} .

The proof (which is constructive) is in Appendix B.1. Applying Lemma 1 with $\alpha = \frac{\gamma}{\epsilon \|\nabla_x J_f(\theta, x, y)\|_2}$, and scaling the obtained unit vectors by ϵ , yields a set of orthogonal perturbations that satisfy $\|r_i\|_2 = \epsilon$ and $r_i^\top \nabla_x J(x, y) = \gamma$, as desired. Informally, the number of orthogonal adversarial directions is proportional to the increase in loss γ (a proxy for the distance from x to the decision boundary) and inversely proportional to the *smoothness* of the loss function and the norm of the perturbation, ϵ . If the value of γ that results in a misclassification is unknown, we attempt the attack with multiple values of γ and use the value of γ that results in the set of orthogonal directions with the most misclassified perturbations. Finding an analog maximal construction of orthogonal perturbations in the ℓ_∞ -norm is an interesting open problem.

Independent JSMA. For discrete features, such as in the DREBIN dataset, it is difficult to find (valid) orthogonal perturbations using the previous methods.

Instead, we propose a simple non-iterative variant of the JSMA for this setting. We compute the saliency map (as in [20]) and rank the features by their saliency scores. Given a target dimensionality k and a maximal perturbation budget B , we group the most salient features into k bins of at most B features each, such that the sum of saliency scores in each bin are roughly equal (we greedily add new features into the non-full bin with lowest total score). As the k sets of features are independent by construction, they naturally yield orthogonal perturbations. We repeat this process for multiple values of k to estimate the dimensionality of the adversarial space.

3.2 Prefiltered Evaluation of the Transfer Rate

To evaluate the transferability from one model to another, we report accuracy in “the prefiltered case,” as done by [12]. That is, we report the accuracy of the target model on adversarial examples that meet two criteria: 1) the original example did not fool the first model, and 2) the adversarial example successfully fools the first model. Departing from the metric used by [12], we also require that 3) the original example did not fool the target model. This evaluation metric focuses on the transferability property rather than effects like natural inaccuracy of the models or failure of the adversarial example construction process. Accuracy in this prefiltered case can be considered the “transfer rate” of the adversarial examples.

3.3 Experiments

The majority of our experiments are performed with a pair of DNNs trained on MNIST. The source model for crafting adversarial examples is a shallow variant of architecture C from Table 3, where we omit two of the four hidden layers. We denote it f_{src} . The target model is the original architecture C with 4 hidden layers, denoted f_{target} . For all methods, we consider perturbations r satisfying $\|r\|_2 \leq 5$. An overview of the results is given in Table 1. We detail the results for each method below.

Second-Order Approximations. This attack is not interesting for rectified linear units, because the Hessian of the logits with respect to the inputs is zero (or undefined) everywhere. In order to study this attack with a nonzero Hessian, we use hyperbolic tangent rather than rectified linear units in the source model. Yet, we still find that H has only small entries and that the optimal solution to the quadratic problem is close to perfectly aligned with the gradient. The best solution that is

orthogonal to the gradient is non-adversarial. Thus, the second-order approximation is of little use in finding further adversarial directions.

Convex Optimization. On the source model f_{src} , the LP yields an adversarial example for 93% of the test inputs. By solving the LP iteratively, we find a little over 2 orthogonal perturbations on average, and 47 for the “most vulnerable” input. As we restrict the search to a region where the model is linear, these orthogonal perturbations span a dense subspace. That is, any perturbation of norm ϵ in the spanned subspace is also adversarial.

However, the transfer rate for these perturbations is low (17% compared to 95% for the FGM). When considering the full adversarial subspace, the transferability increases only marginally: for 70% of the inputs, none of the successful perturbations on model f_{src} transfers to model f_{target} . Thus, although the LP approach may find smaller adversarial perturbations and in more directions than methods such as FGM [3], we also find that it is less effective at yielding transferable perturbations.²

Gradient Aligned Adversarial Subspace. The GAAS method was the most successful at finding a large number of orthogonal attack directions. This gives further evidence that neural networks generalize in an eerily linear fashion to out-of-sample data, as first hypothesized in [8].

In Figure 2, we plot the probability density function of the dimensionality of the adversarial subspace for each input. On average, we find 44.28 orthogonal perturbations (and more than 200 for the most vulnerable inputs) and 24.87 directions that transfer to model f_{target} . These perturbations span a dense subspace of adversarial inputs: by randomly sampling a perturbation in the spanned space (with an ℓ_2 -norm of 5.0), we fool model f_{src} in 99% of cases, and model f_{target} in 89% of cases.

We repeat the experiment for two CNN’s (model B in Table 3 as source, and A as target). The transfer rate for the FGM is lower for these models (68%). We find fewer orthogonal perturbations on the source model (15.18), and, expectedly, fewer that transfer (2.24). With high probability, points in the spanned adversarial subspace mislead the source (80%) and target (63%) models.

Independent JSMA. We evaluated the JSMA variant on the DREBIN dataset, for the same DNN models as above. With a maximal budget of 10 flipped features per perturbation, we find at least one successful perturbation for 89% of the inputs, and 42 successful independent perturbations on average. Of these, 22 transfer to the target model.

Although we did not verify that all these perturbations truly retain the (non)-malicious nature of the input program, we note that flipping a *random* subset of 10 input features does not cause the models to misclassify at a higher rate than on clean data. As our pre-processing of the DREBIN dataset selects those features that have a large impact on classification (and thus are often useful to adversaries), we don’t expect the number of independent perturbations to increase significantly for variants of DREBIN with larger feature dimensionality.

4 Decision Boundary Similarity enables Transferability

Evidenced by Section 3, the existence of large subspaces of transferable adversarial examples suggests that the decision boundaries learned by both the source and target models must be close to one another in the direction given by the adversarial gradient.

In this section, we quantitatively characterize the similarity between decision boundaries in both adversarial and benign directions. Our measurements show that when moving away from data points in any particular direction, the distance between two models’ decision boundaries is usually smaller than the distance separating the data points from either boundary.

Furthermore, we find that adversarial training [23] does not significantly “displace” the learned decision boundary, which could explain why adversarially trained models have been observed to remain vulnerable to black-box attacks [19].

²The approach of Bastani et al. [3] sometimes fails to produce adversarial examples. For instance, for architecture C in Table 3 and perturbations $\|r\|_2 \leq 5$, the obtained LP is solvable for 0% of tested inputs, whereas the FGSM always yields a successful adversarial example.

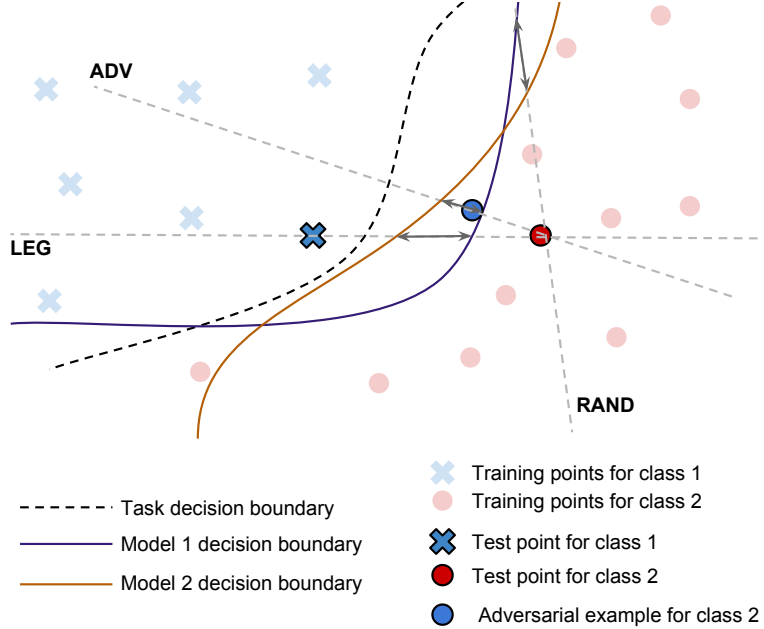


Figure 3: The three directions (Legitimate, Adversarial and Random) used throughout Section 4 to measure the distance between the decision boundaries of two models. The gray double-ended arrows illustrate the *inter-boundary* distance between the two models in each direction.

4.1 Distance Definitions

In the absence of closed-form expressions, evaluating the decision boundary of a ML model with high-dimensionality is intractable. We thus restrict ourselves to measuring similarity in three linear directions, chosen for being representative of the model behavior on and off the data manifold.

Directions. The definition of the three directions is illustrated in Figure 3 with a binary classification task over a 2D input domain. In addition, each direction is formally defined below as a unit-norm vector relative to a data point x that is part of the legitimate test data X_t and another point x' :

$$\vec{d}(f, x) := \frac{x' - x}{\|x' - x\|_2} \quad (2)$$

Distance is measured using the ℓ_2 norm (we present similar results with the ℓ_1 norm in Appendix C). The point x' is defined differently for each direction, as follows:

1. **Legitimate direction**—Written $\vec{d}_{\text{leg}}(f, x)$, it is defined by x and the closest test data point $x' \in X_t$ with a different class label than x .
2. **Adversarial direction**—Written $\vec{d}_{\text{adv}}(f, x)$, it is defined by x and an adversarial example $x' := \text{adv}(f, x)$ generated from x to be misclassified by f .
3. **Random direction**—Written $\vec{d}_{\text{rand}}(f, x)$, it is defined by x and an input x' drawn uniformly over the input domain. We repeatedly sample the point x' until it is classified by f in a different class than x (with a limit of 100 tries).

These directions are used to define two types of metrics:

Minimum Distances. The first type is a set of *minimum distances*. They quantify the perturbation required to project a test input onto a model’s decision boundary. Given one of the above directions \vec{d} , the *minimum distance* from a point x to the model’s decision boundary is defined as:

$$\text{MIN-DIST}_{\vec{d}}(f, x) := \arg \min_{\epsilon > 0} f(x + \epsilon \cdot \vec{d}) \neq f(x) . \quad (3)$$

Inter-Boundary Distances. We are however interested in measuring the *distance between the decision boundaries* of different models in these directions (i.e., the bi-directional arrows in Figure 3). Our second set of metrics are therefore *inter-boundary distances*, that measure the distance between the projections of a point onto the decision boundaries of two distinct models. Specifically, for a point x and a direction \vec{d} computed according to f_1 (e.g., $\vec{d} = \vec{d}_{\text{adv}}(f_1, x)$), we define the *inter-boundary distance* between f_1 and f_2 as:

$$\text{INTER-DIST}_{\vec{d}}(f_1, f_2, x) := |\text{MIN-DIST}_{\vec{d}}(f_1, x) - \text{MIN-DIST}_{\vec{d}}(f_2, x)|. \quad (4)$$

The *inter-boundary distance* in the adversarial direction is directly related to adversarial example transferability: If the distance is small, adversarial examples crafted from f_1 that cross the decision boundary of f_1 are likely to also cross the decision boundary of f_2 (hence, they *transfer*). Note that the inter-boundary distance is usually *not symmetric*, as the considered distance \vec{d} is computed with respect to the “source” model f_1 .

4.2 Experiments with the MNIST and DREBIN Datasets

We study three models trained on the MNIST and DREBIN tasks: a logistic regression (LR), support vector machine (SVM), and neural network (DNN architecture C in Table 3). For all pairs of models, we compute the inter-boundary distance in the three directions: legitimate, adversarial and random. The minimum distance in the same direction acts as a baseline for these values.

When the inter-boundary distance is much smaller than the minimum distance in the adversarial direction, it follows that adversarial examples will transfer—so long as they did not lie exactly on the decision boundary of the model they were crafted with. In addition, if the inter-boundary distance is also an order of magnitude smaller than the minimal distance in the legitimate or random directions, then this illustrates proximity of model decision boundaries on and off the data manifold.

Experimental Setup. All input domain distances are measured with the ℓ_2 norm. When reporting a particular distance measurement, we report the average distance for all points in the test set. We determine adversarial directions with the FGM [8] for differentiable models (the LR and DNN) and the method introduced in [18] for the SVM. Note that since we are working with the ℓ_2 norm, we employ the corresponding variant of the FGM described in Section 2. To compute the minimum distance from a point to a decision boundary in a particular direction, we use a line search with step size 0.05. We do not round DREBIN features to their closest binary value—in contrast to what was done in Section 3. If we did, the line search would become too coarse-grained and yield less accurate measurements of the distances separating decision boundaries.

Figure 4 shows the results for the MNIST dataset. In the interest of space, further results are deferred to the Appendix. These include MNIST results with the ℓ_1 norm, as well as results on DREBIN. The observations made below hold for those experiments as well.

Minimum Distance Measurements. Distances to the decision boundary are indicated by filled black bars in Figure 4. As expected, the distance is smallest in the adversarial direction. In addition, we observe that decision boundaries are further away in the random direction than in the one of another legitimate test input classified in a different class. This corroborates with the observation that random noise does not usually cause misclassification [23].

Inter-Boundary Distances. We now compare inter-boundary distances (hatched bars) with minimum distances (filled black bars). For most pairs of models and directions, the minimum distance from a test input to the decision boundary is larger than the distance between the decision boundaries of the two models in that direction. For the adversarial direction, this confirms our hypothesis for the existence of transferability: for an adversarial example to transfer, the perturbation magnitude needs to be only slightly larger than the minimum perturbation required to fool the source model.

We find that the results for our experiments using the SVM as source model are quantitatively different (i.e., the inter-boundary distances in the adversarial directions are considerably larger in this case). This is most likely due to our SVM implementation using a “one-vs-rest” strategy, which yields a slightly different optimization problem for crafting adversarial examples.

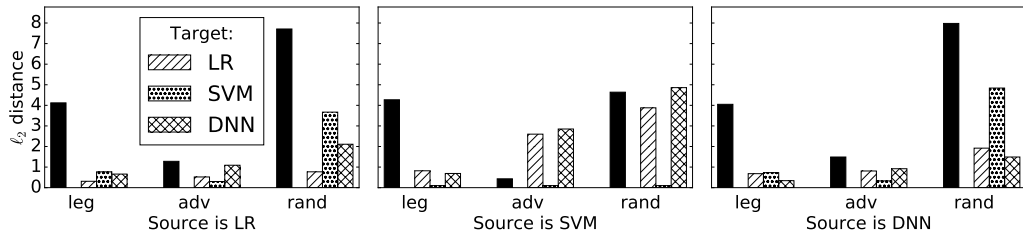


Figure 4: Minimum distances and inter-boundary distances in three directions between models trained on MNIST. Each plot shows results for one source model, and all three classes of target models (one hatched bar per model class). Within each plot, bars are grouped by direction (legitimate, adversarial and random). The filled black bar shows the minimum distance to the decision boundary, computed on the source model. The adversarial search uses the FGM with $\varepsilon = 5$.

The fact that the inter-boundary distances are smaller than the minimum distances, even in the legitimate and random directions, suggests that the models’ decision boundaries are close to one another both on and off the data manifold.

4.3 Impact of Adversarial Training on the Distance between Decision Boundaries

In the previous experiments, we saw how similarity between decision boundaries enables transferability of adversarial examples across models. Surprisingly, it has been shown in [19] that adversarial examples tend to transfer even in the presence of explicit (and at a first glance successful) defenses against adversarial examples, such as adversarial training [8] or defensive distillation [22]. This suggests that these defenses do not significantly “displace” a model’s decision boundaries (and thus only marginally improve its robustness). Rather, it appears that these defenses succeed at preventing *white-box* attacks by reducing the reliability of first-order approximations used for crafting adversarial examples (an effect known as gradient masking [21]). We leave an investigation of the interplay of transferability and adversarial training to future work.

We repeat the measurements of minimal and inter-boundary distances with a pair of DNNs, one of which is adversarially trained. We use the undefended model as source, and target the adversarially trained model. For all directions (legitimate, adversarial and random), we find that the inter-boundary distance between the source and target models is increased compared to the baseline in Figure 4.

However, the increase is too little for transferability to be eliminated: In the adversarial direction, the average inter-boundary distance increases from 0.32 (when the target is undefended) to 0.63 (when the target is adversarially trained), yet remains smaller than the minimal adversarial perturbation on the source model (1.64). Thus, adversarial perturbations with sufficient magnitude to “overshoot” the decision boundary of the source model still transfer to the adversarially trained model.

5 Limits of Transferability

Recall the hypothesis on the ubiquity of transferability formulated in the Introduction:

If two models achieve low error for some task while also exhibiting low robustness to adversarial examples, these adversarial examples transfer between the models.

We first derive conditions on the data distribution under which a form of this hypothesis holds. However, we also show a counter-example: a specific task for which adversarial examples do not transfer between linear and quadratic models. This suggests that transferability is not an inherent property of non-robust ML models and that it may be possible to prevent black-box attacks (at least for some model classes) despite the existence of adversarial examples.³

³We consider here an adversary that attacks a target model by transferring adversarial examples crafted on a locally trained model. Note that if the adversary can mount a model theft attack [19, 24] that recovers a close approximation of the target model, then any model vulnerable in a white-box setting can be attacked.

5.1 Sufficient Conditions for Transferability

We exhibit some *sufficient conditions* under which a specific type of adversarial perturbation transfers from input space to richer feature spaces in binary classification tasks. These perturbations are *model agnostic*; they shift data points in the direction given by the *difference between the intra-class means*.

We consider binary classifiers $f(x) = w^\top \phi(x) + b$ defined as the composition of an arbitrary feature mapping $\phi(x)$ and a linear classifier. These include linear models, polynomial models and feed-forward neural networks (where ϕ is defined by all but the last layer of the network). The expected 0-1 loss of f over some data distribution μ is denoted $L(f) := \Pr_\mu(\text{sign}(f(x)) \neq y)$.

Under natural assumptions, any linear classifier with low risk will be fooled by perturbations in the direction of the difference in class means (this follows from a result by Fawzi et al. [7]). Moreover, for classifiers with a richer feature set (e.g. quadratic classifiers), we relate robustness to this perturbation to the extent in which *the direction between the class means in input space is preserved in feature space*. This is a property solely of the data distribution and feature mapping considered i.e., it is independent of any specific classifier.

Model-Agnostic Perturbations. For a fixed feature mapping ϕ , we consider the perturbation (in feature space) that shifts data points in the direction given by the difference in intra-class means. Let

$$\delta_\phi := \frac{1}{2} \cdot (\mathbb{E}_{\mu_{+1}}[\phi(x)] - \mathbb{E}_{\mu_{-1}}[\phi(x)]) . \quad (5)$$

where μ_{-1} and μ_{+1} respectively denote the data distributions of the positive and negative class. For an input (x, y) , we define the feature-space perturbation $r_\phi := -\epsilon \cdot y \cdot \hat{\delta}_\phi$, where \hat{v} denotes a non-zero vector v normalized to unit norm. For large ϵ , the feature-space perturbation $\phi^*(x) = \phi(x) + r_\phi$ will fool any model f if the weight vector w is aligned with the difference in class means δ_ϕ , i.e. we have:

$$\Delta := \hat{w}^\top \hat{\delta}_\phi > 0 . \quad (6)$$

For certain tasks and model classes, we show that this assumption must hold for f to obtain low error. Following [7], we need $\epsilon \approx \|\delta_\phi\|_2$ on average for f to misclassify (see Appendix B.2 for details). For tasks with close class means (e.g., most vision tasks, see [7]), the perturbation is likely adversarial.

We now ask to what extent model-agnostic perturbations in *input space* will transfer to models over richer feature spaces. Let δ and r denote, respectively, the difference in means, and the model-agnostic perturbation in input space, i.e.,

$$\delta := \frac{1}{2}(\mathbb{E}_{\mu_{+1}}[x] - \mathbb{E}_{\mu_{-1}}[x]) \quad , \quad r := -\epsilon \cdot y \cdot \hat{\delta} . \quad (7)$$

Under the assumption that the weight vector is aligned with the difference in class means, a sufficient condition for transferability is that r is mapped by ϕ to a perturbation that is closely aligned with the difference in class means *in feature space*, i.e.,

$$\phi(x + r) \approx \phi(x) + r_\phi . \quad (8)$$

When a mapping ϕ satisfies this, we say it is *pseudo-linear* in r . We now state our result, informally:

Theorem 2 (Informal). *Let $f(x) = w^\top \phi(x) + b$, with ϕ some feature mapping. Let r be a perturbation aligned with the difference in class means δ . If the angle $\Delta := \hat{w}^\top \hat{\delta}_\phi$ is not too small, e.g., $\Delta \gg L(f)$, and ϕ is “pseudo-linear” in r , then adversarial examples $x + r$ will transfer to model f .*

The detailed statement of the theorem is in Theorem 3. We defer it and its proof to the Appendix B.2.

Experiments on MNIST. We empirically assess the validity of our analysis on the binary task of distinguishing 3’s and 7’s from the MNIST dataset. We use linear models, quadratic models ($f(x) = x^\top Ax + b$, where A is a symmetric matrix), DNNs and CNNs. All models have the form $f(x) = w^\top \phi(x) + b$ for some appropriate mapping ϕ .

All models satisfy the assumption in Equation (6): the linear model in feature space is strongly aligned with the difference in class means. In fact, by keeping the feature map fixed and varying w , we find that any linear or quadratic model that does not satisfy this assumption has low accuracy.



Figure 5: MNIST digits perturbed by adding the difference in class means.

Model	Acc.	Acc. on shifted data	Δ	ϕ satisfies pseudo-linearity in r
Linear	98.2%	39%	0.55	Yes
Quadratic	99.3%	51%	0.51	Yes
DNN	99.3%	43%	0.68	Yes
CNN	99.9%	76%	0.79	No

Table 2: Results for the model agnostic adversarial perturbation that shifts points in the direction of the difference in class means. We used $\epsilon = 4$, for r as defined in (7). The angle Δ is measured between the weights w of the final linear layer and the difference in class means in feature space, δ_ϕ .

We use the mean-shift perturbation r defined in (7) with $\epsilon = 4$. Examples of perturbed inputs are in Figure 5; the correct labels are self-evident despite the appearance of a faint “ghost” digit in some images. Table 2 reports the accuracy of each model on clean data and the perturbed inputs. All models are partially fooled by this small model-agnostic perturbation.

In addition, Table 2 reports whether each model satisfies the technical conditions of Theorem 2 (i.e., the *pseudo-linearity* of mapping ϕ with respect to the perturbation r). Since the quadratic feature mapping satisfies these conditions, *any* quadratic classifier with high accuracy (and thus positive alignment between w and δ_ϕ) will be at least in part vulnerable to the considered perturbations. Thus, *any accurate pair of linear and quadratic classifiers for this task will exhibit transferability*. This can be seen as a special case of the hypothesis discussed at the beginning of this Section.

The pseudo-linearity condition does not hold for the CNN: the perturbation direction is not sufficiently preserved in feature space for our result to hold unconditionally. However, our bounds are (expectedly) somewhat loose and we find that the CNN still misclassifies 24% of perturbed samples.

To generalize this approach to multi-class settings, we can define perturbations through pairwise differences in means: $\mathbb{E}_{\mu_i}[x] - \mathbb{E}_{\mu_j}[x]$, where x has label $y = i$, and $j \neq i$ is a chosen target class. We can also use the ℓ_∞ norm, by setting $r := -\epsilon \cdot \text{sign}(\mathbb{E}_{\mu_i}[x] - \mathbb{E}_{\mu_j}[x])$. With this adversarial perturbation (for $\epsilon = 0.3$) the same model architectures trained on the full MNIST dataset attain accuracy between 2% (for the linear model) and 66% (for the CNN).

Experiments on DREBIN. We evaluated the same model-agnostic perturbations on the DREBIN dataset. It is noteworthy that on DREBIN, the class mean is less semantically meaningful than on MNIST (i.e., the mean feature vector of all malware applications is unlikely to even belong to the input space of valid programs). Yet, the same perturbation (followed by rounding to binary features) reliably fools both a linear model and a DNN. By modifying fewer than 10 of the 1000 binary features on average, the accuracy of the linear model drops to 65% and that of the DNN to 72%.

5.2 XOR Artifacts

The previous analysis showed that transferability can be inherent if models are defined on (or learn) feature representations that preserve non-robust input-space features. We now show that if models were to learn very different sets of (possibly non-robust) features, transferability need not hold.

As a thought-experiment, for a given dataset, consider two models trained on *independent subsets* of the input features. In this setting, adversarial examples crafted to specifically mislead one of the models would not transfer to the other. However, it is expected that adversarial examples crafted on a model trained over the full feature set would still transfer to both models.

Hereafter, we ask a more realistic question: for a given task, can models with access to the *same set of input features* learn representations for which adversarial examples do not transfer to one another—even when these models are not robust to their own adversarial examples. We provide a simple example of a task for which this is true.



Figure 6: MNIST digits with an additional XOR artifact. Best viewed zoomed in and in color. Blue pixels are positive, red pixels are negative.

We first train linear and quadratic models on the same binary MNIST task (3s vs. 7s). Both models get over 98% accuracy. FGM examples (with $\|r\|_2 = 4$) transfer between the models at a rate above 60%. We then consider a variant of this dataset with pixels taking values in \mathbb{R}^d rather than $[0, 1]^d$. We add a special “XOR artifact” to images: for two of the center pixels, images of 3s contain a negative XOR (i.e., one of the pixels has positive value, the other negative), and images of 7s contain a positive XOR (both pixels have either positive or negative value). Some examples are shown in Figure 6. Intuitively, this alteration will be ignored by the linear model (the artifact is not linearly separable) but not by the quadratic model as the XOR product is a perfect predictor.

Both models trained on this data remain vulnerable to small, *but different*, adversarial perturbations. The linear model is fooled by standard FGM examples and the quadratic model is fooled by flipping the sign of the two center pixels. Neither of these perturbations transfers to the other model. Fooling both models simultaneously requires combining the perturbations for each individual model.

Our experiment on this artificially altered dataset demonstrates how different model classes may learn very different concepts that, while strongly predictive, have little correspondence with our visual perception of the task at hand. It is interesting to consider whether any real datasets might exhibit a similar property, and thus result in learned models exhibiting low transferability.

Acknowledgments

We thank Ben Poole and Jacob Steinhardt for feedback on early versions of this work. Nicolas Papernot is supported by a Google PhD Fellowship in Security. Research was supported in part by the Army Research Laboratory, under Cooperative Agreement Number W911NF-13-2-0045 (ARL Cyber Security CRA), and the Army Research Office under grant W911NF-13-1-0421. The views and conclusions contained in this document are those of the authors and should not be interpreted as representing the official policies, either expressed or implied, of the Army Research Laboratory or the U.S. Government. The U.S. Government is authorized to reproduce and distribute reprints for government purposes notwithstanding any copyright notation hereon.

References

- [1] Daniel Arp, Michael Spreitzenbarth, Malte Hubner, Hugo Gascon, Konrad Rieck, and CERT Siemens. Drebin: Effective and explainable detection of android malware in your pocket. In *NDSS*, 2014.
- [2] Marco Barreno, Blaine Nelson, Russell Sears, Anthony D Joseph, and J Doug Tygar. Can machine learning be secure? In *Proceedings of the 2006 ACM Symposium on Information, computer and communications security*, pages 16–25. ACM, 2006.
- [3] Osbert Bastani, Yani Ioannou, Leonidas Lampropoulos, Dimitrios Vytiniotis, Aditya Nori, and Antonio Criminisi. Measuring neural net robustness with constraints. In *Advances In Neural Information Processing Systems*, pages 2613–2621, 2016.
- [4] Vahid Behzadan and Arslan Munir. Vulnerability of deep reinforcement learning to policy induction attacks. *arXiv preprint arXiv:1701.04143*, 2017.
- [5] Battista Biggio, Iginio Corona, Davide Maiorca, Blaine Nelson, Nedim Šrđić, Pavel Laskov, Giorgio Giacinto, and Fabio Roli. Evasion attacks against machine learning at test time. In *Joint European Conference on Machine Learning and Knowledge Discovery in Databases*, pages 387–402. Springer, 2013.
- [6] Battista Biggio, Blaine Nelson, and Pavel Laskov. Poisoning attacks against support vector machines. *arXiv preprint arXiv:1206.6389*, 2012.
- [7] Alhussein Fawzi, Omar Fawzi, and Pascal Frossard. Analysis of classifiers’ robustness to adversarial perturbations. *arXiv preprint arXiv:1502.02590*, 2015.

- [8] Ian J Goodfellow, Jonathon Shlens, and Christian Szegedy. Explaining and harnessing adversarial examples. *arXiv preprint arXiv:1412.6572*, 2014.
- [9] Kathrin Grosse, Nicolas Papernot, Praveen Manoharan, Michael Backes, and Patrick McDaniel. Adversarial perturbations against deep neural networks for malware classification. *arXiv preprint arXiv:1606.04435*, 2016.
- [10] Weiwei Hu and Ying Tan. Generating adversarial malware examples for black-box attacks based on gan. *arXiv preprint arXiv:1702.05983*, 2017.
- [11] Sandy Huang, Nicolas Papernot, Ian Goodfellow, Yan Duan, and Pieter Abbeel. Adversarial attacks on neural network policies. *arXiv preprint arXiv:1702.02284*, 2017.
- [12] Alexey Kurakin, Ian Goodfellow, and Samy Bengio. Adversarial examples in the physical world. *arXiv preprint arXiv:1607.02533*, 2016.
- [13] Pavel Laskov et al. Practical evasion of a learning-based classifier: A case study. In *Security and Privacy (SP), 2014 IEEE Symposium on*, pages 197–211. IEEE, 2014.
- [14] Yann LeCun, Léon Bottou, Yoshua Bengio, and Patrick Haffner. Gradient-based learning applied to document recognition. *Proceedings of the IEEE*, 86(11):2278–2324, 1998.
- [15] Yen-Chen Lin, Zhang-Wei Hong, Yuan-Hong Liao, Meng-Li Shih, Ming-Yu Liu, and Min Sun. Tactics of adversarial attack on deep reinforcement learning agents. *arXiv preprint arXiv:1703.06748*, 2017.
- [16] Yanpei Liu, Xinyun Chen, Chang Liu, and Dawn Song. Delving into transferable adversarial examples and black-box attacks. *arXiv preprint arXiv:1611.02770*, 2016.
- [17] Nicolas Papernot, Ian Goodfellow, Ryan Sheatsley, Reuben Feinman, and Patrick McDaniel. cleverhans v1.0.0: an adversarial machine learning library. *arXiv preprint arXiv:1610.00768*, 2016.
- [18] Nicolas Papernot, Patrick McDaniel, and Ian Goodfellow. Transferability in machine learning: from phenomena to black-box attacks using adversarial samples. *arXiv preprint arXiv:1605.07277*, 2016.
- [19] Nicolas Papernot, Patrick McDaniel, Ian Goodfellow, Somesh Jha, Z Berkay Celik, and Ananthram Swami. Practical black-box attacks against deep learning systems using adversarial examples. *arXiv preprint arXiv:1602.02697*, 2016.
- [20] Nicolas Papernot, Patrick McDaniel, Somesh Jha, Matt Fredrikson, Z Berkay Celik, and Ananthram Swami. The limitations of deep learning in adversarial settings. In *Security and Privacy (EuroS&P), 2016 IEEE European Symposium on*, pages 372–387. IEEE, 2016.
- [21] Nicolas Papernot, Patrick McDaniel, Arunesh Sinha, and Michael Wellman. Towards the science of security and privacy in machine learning. *arXiv preprint arXiv:1611.03814*, 2016.
- [22] Nicolas Papernot, Patrick McDaniel, Xi Wu, Somesh Jha, and Ananthram Swami. Distillation as a defense to adversarial perturbations against deep neural networks. In *Security and Privacy (SP), 2016 IEEE Symposium on*, pages 582–597. IEEE, 2016.
- [23] Christian Szegedy, Wojciech Zaremba, Ilya Sutskever, Joan Bruna, Dumitru Erhan, Ian Goodfellow, and Rob Fergus. Intriguing properties of neural networks. *arXiv preprint arXiv:1312.6199*, 2013.
- [24] Florian Tramèr, Fan Zhang, Ari Juels, Michael K Reiter, and Thomas Ristenpart. Stealing machine learning models via prediction apis. In *Usenix Security*, 2016.
- [25] David Warde-Farley and Ian Goodfellow. Adversarial perturbations of deep neural networks. In *Advanced Structured Prediction*. 2016.
- [26] Weilin Xu, Yanjun Qi, and David Evans. Automatically evading classifiers. In *Proceedings of the 2016 Network and Distributed Systems Symposium*, 2016.

A Neural Network Architectures

Model ID		
A	B	C
Conv(64, 5, 5) + Relu	Dropout(0.2)	$\left[\begin{array}{l} \text{FC}(300) + \text{Relu} \\ \text{Dropout}(0.5) \end{array} \right] \times 4$ FC + Softmax
Conv(64, 5, 5) + Relu	Conv(64, 8, 8) + Relu	
Dropout(0.25)	Conv(128, 6, 6) + Relu	
FC(128) + Relu	Conv(128, 5, 5) + Relu	
Dropout(0.5)	Dropout(0.5)	
FC + Softmax	FC + Softmax	

Table 3: Neural network architectures used in this work. Conv: convolutional layer, FC: fully connected layer.

B Proofs

B.1 Proof of Lemma 1

We begin with the upper bound. Let $\hat{r}_i := \frac{r_i}{\|r_i\|_2}$. Then, note that if r_1, r_2, \dots, r_k are orthogonal, we have

$$\|g\|_2^2 \geq \sum_{i=1}^k |g^\top \hat{r}_i|^2 \geq \sum_{i=1}^k \frac{|g^\top x_i|^2}{\|r_i\|_2^2} \geq k \cdot \alpha^2 \cdot \|g\|_2^2,$$

which implies $k \leq \lfloor \frac{1}{\alpha^2} \rfloor$. If $\alpha < \frac{1}{\sqrt{d}}$, the bound $k \leq d$ is trivial.

We prove the lower bound with a concrete construction of the vectors r_i . Let e_1, e_2, \dots, e_d denote the basis vectors in \mathbb{R}^d . Let $k = \lfloor \frac{1}{\alpha^2} \rfloor \leq d$ and denote by R a rotation matrix that satisfies $Rg = \|g\|_2 \cdot e_1$ (i.e., R rotates vectors into the direction given by g). Let $z := \sum_{i=1}^k k^{-\frac{1}{2}} \cdot e_i$, and let S be the rotation matrix that satisfies $Sz = e_1$. Then, it is easy to see that $Q := S^\top R$ is a rotation matrix that satisfies $Qg = \|g\|_2 \cdot z$.

The vectors $r_i := Q^\top e_i$ for $1 \leq i \leq k$ (these are the first k rows of Q) are orthonormal, and satisfy $g^\top r_i = \|g\|_2 \cdot z^\top e_i = \|g\|_2 \cdot k^{-\frac{1}{2}} \geq \|g\|_2 \cdot \alpha$.

B.2 Proof of Theorem 2

We first formally define the notion of *pseudo-linearity*. For the input-space perturbation r and a feature mapping ϕ , consider the orthogonal decomposition

$$\phi(x+r) - \phi(x) = \alpha \cdot \delta_\phi + \beta \cdot \delta_\phi^\perp, \tag{9}$$

where δ_ϕ^\perp is orthogonal to δ_ϕ and of equal norm (i.e., $\|\delta_\phi^\perp\|_2 = \|\delta_\phi\|_2$).

Intuitively, for the perturbation in the direction of the difference in means to be preserved in feature space, we want α to be large, and β to be not too large. This is what we informally mean by ϕ being *pseudo-linear* in r . The precise statement of our Theorem is then:

Theorem 3 (Full Version of Theorem 2). *Let $f(x) = w^\top \phi(x) + b$, where ϕ is a fixed feature mapping. Let r be a perturbation aligned with the difference in class means δ . If the angle $\Delta := \hat{w}^\top \hat{\delta}_\phi$ is not too small, e.g., $\Delta \gg L(f)$, and $\mathbb{E}_\mu(-y\alpha) \geq 1 + \frac{1-\Delta}{\Delta} \mathbb{E}_\mu(|\beta|)$, then adversarial examples $x+r$ will transfer to model f with non-zero probability.*

Proof. We begin by deriving the average ℓ_2 -norm of the perturbation r_ϕ in feature space, so that f misclassifies *all* inputs. Without loss of generality, we assume that $b < \max_{x \in \mu} |w^\top \phi(x)|$ (i.e., the sign of the classifier is not constant).

Lemma 4. Let $f = w^\top \phi(x) + b$ with $L(f) < \frac{1}{2}$ and $\Delta := \hat{w}^\top \hat{\delta}_\phi > 0$. For any $x \in D$, let r_ϕ be the smallest (in ℓ_2 -norm) perturbation aligned with δ_ϕ , such that $\text{sign}(w^\top(\phi(x) + r)) \neq y$. Then,

$$\mathbb{E}_\mu(\|r_\phi\|_2) \leq \|\delta_\phi\|_2 + \frac{4 \cdot L(f) \cdot \max_{x \in D} \|\phi(x)\|_2}{\Delta}.$$

Proof. Recall that $\delta_\phi = \frac{1}{2} \cdot (\mathbb{E}_{\mu_{+1}}[\phi(x)] - \mathbb{E}_{\mu_{-1}}[\phi(x)])$. If x is misclassified by f , then $\|r_\phi\|_2 = 0$. Otherwise, it is easy to see that

$$\|r_\phi\|_2 = \frac{|f(x)|}{w^\top \delta_\phi} \cdot \|\delta_\phi\|_2.$$

A simple adaption of the analysis of Fawzi et al. [7] (for the case of linear models) yields

$$\mathbb{E}_\mu[|f(x)|] \leq w^\top \delta_\phi + 4 \cdot L(f) \cdot \|w\|_2 \cdot \max_{x \in \mu} \|\phi(x)\|_2.$$

Combining these results, we obtain

$$\begin{aligned} \mathbb{E}_\mu(\|r_\phi\|_2) &\leq \|\delta_\phi\|_2 + 4 \cdot L(f) \cdot \max_{x \in \mu} \|\phi(x)\|_2 \cdot \frac{\|w\|_2 \cdot \|\delta_\phi\|_2}{w^\top \delta_\phi} \\ &= \|\delta_\phi\|_2 + \frac{4 \cdot L(f) \cdot \max_{x \in \mu} \|\phi(x)\|_2}{\Delta} \end{aligned}$$

□

Lemma 4 is an extension of the result of Fawzi et al. [7], who show that if the difference in class means is small, any linear model with low risk can be fooled by small perturbations along the direction of w . Because we are interested in the simple “model-agnostic” perturbation that directly follows the difference of means, the magnitude of the perturbation further depends on the alignment Δ between w and δ_ϕ , which is positive according to the assumption in Equation (6).

We now consider transferability of the perturbation r in input space. Recalling (9), we can write

$$w^\top \phi(x + r) = w^\top (\phi(x) + \alpha \cdot \delta_\phi + \beta \cdot \delta_\phi^\perp)$$

Assume $\Delta \gg L(f)$ and suppose first that $\beta = 0$. Then, according to Lemma 4, on average, the minimal value of $(-y \cdot \alpha)$ to get f to misclassify is ≈ 1 . However, the contribution of $\beta \cdot \delta_\phi^\perp$ has to be taken into account. Note that $\hat{w}^\top \hat{\delta}_\phi^\perp \leq 1 - \Delta$. Thus, we have

$$|\beta \cdot w^\top \delta_\phi^\perp| \leq |\beta| \cdot \|w\|_2 \cdot \|\delta_\phi\| \cdot (1 - \Delta).$$

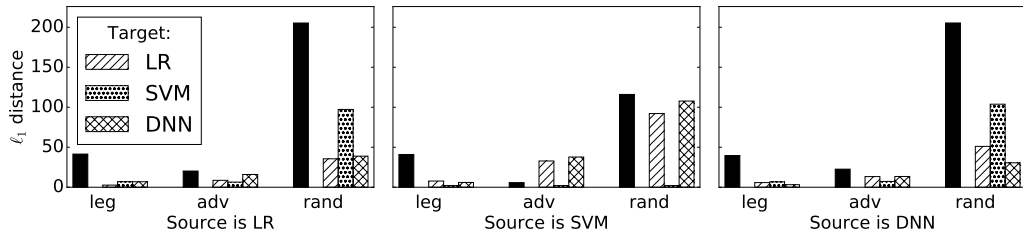
In the worst case, the absolute magnitude of α should be increased by $\frac{1-\Delta}{\Delta} |\beta|$ to ensure that any non-adversarial contribution of the orthogonal component of the perturbation is canceled out. Thus, in expectation, we need $-y \cdot \alpha \geq 1 + \frac{1-\Delta}{\Delta} |\beta|$ to have f misclassify with non-zero probability. Note that this bound is expected to be loose in practice, as the orthogonal component δ_ϕ^\perp is unlikely to be maximally aligned with w .

□

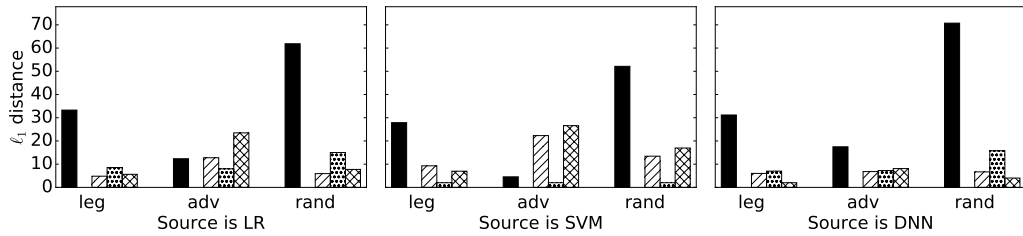
C Appendix: Additional Distance Measurements

We provide additional measurements of the similarity in models’ decision boundaries.

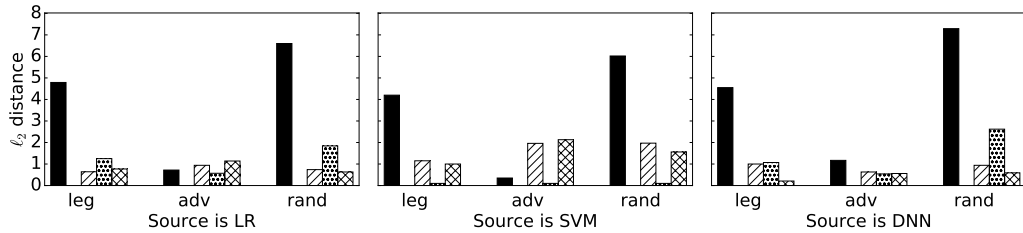
Inter-boundary distances computed on the MNIST models with the ℓ_1 norm are reported in Figure 7a. Results for the ℓ_2 norm appeared in Figure 4. Analog results for the DREBIN models are reported in Figure 7b and 7c.



(a) Distances measured using the ℓ_1 norm for the MNIST models. The adversarial search uses $\varepsilon = 80$.



(b) Distances measured using the ℓ_1 norm for the DREBIN models. The adversarial search uses $\varepsilon = 80$.



(c) Distances measured using the ℓ_2 norm for the DREBIN models. The adversarial search uses $\varepsilon = 5$.

Figure 7: Minimum distances and inter-boundary distances in three directions between models trained on MNIST and DREBIN. Each plot shows results for one source model, and all three classes of target models (one hatched bar per model class). Within each plot, bars are grouped by direction (legitimate, adversarial and random). The filled black bar shows the minimum distance to the decision boundary, computed on the source model. The adversarial search uses the FGM in either the ℓ_1 or ℓ_2 norm.